haematologica
Journal of The Ferrata Storti Foundation

Targeting shear gradient activated von Willebrand factor by the novel single-chain antibody A1 reduces occlusive thrombus formation *in vitro*

by Thomas Hoefer, Akshita Rana, Be'eri Niego, Shweta Jagdale, Hugo J. Albers, Elizabeth E. Gardiner, Robert K. Andrews, Andries D. van der Meer, Christoph E. Hagemeyer and Erik Westein

Haematologica 2020 [Epub ahead of print]

Citation: Thomas Hoefer, Akshita Rana, Be'eri Niego, Shweta Jagdale, Hugo J. Albers, Elizabeth E. Gardiner, Robert K. Andrews, Andries D. van der Meer, Christoph E. Hagemeyer and Erik Westein. Targeting shear gradient activated von Willebrand factor by the novel single-chain antibody A1 reduces occlusive thrombus formation in vitro. Haematologica. 2020; 105:xxx doi:10.3324/haematol.2020.250761

Targeting shear gradient activated von Willebrand factor by the novel single-chain antibody A1 reduces occlusive thrombus formation in vitro.

Thomas Hoefer[1*], Akshita Rana[2*], Be'eri Niego[2], Shweta Jagdale[1,2], Hugo J. Albers[3,4], Elizabeth E. Gardiner[5], Robert K. Andrews[2], Andries D. van der Meer[3], Christoph E. Hagemeyer[1,2**]& Erik Westein[1,2**]

[1]Baker Heart and Diabetes Institute, Melbourne, Australia;
[2]Australian Centre for Blood Diseases, Monash University, Melbourne, Australia;
[3]Applied Stem Cell Technologies, University of Twente, Enschede, The Netherlands;
[4]BIOS Lab-on-a-Chip, University of Twente, Enschede, The Netherlands;
[5]ACRF Department of Cancer Biology and Therapeutics, John Curtin School of Medical Research, Australian National University, Canberra, Australia

Short title: Targeting VWF to inhibit occlusive thrombus formation

* TH and AR contributed equally to this work

**CEH and EW contributed equally to this work

Address for correspondence:
Erik Westein, PhD
Monash University
Australian Centre for Blood Diseases
89 Commercial Road
Melbourne VIC 3004, Australia
Email: erik.westein@monash.edu

Keywords: von Willebrand Factor, shear stress gradients, thrombosis

Subject codes: thrombosis

Word count abstract: 249
Word count body: 4615

Total number of Figures and Tables: 5 (plus 2 supplementary figures)

TOC Category: Translational

TOC subcategory: Thrombosis

Abstract:

Intraluminal thrombus formation precipitates conditions such as acute myocardial infarction and disturbs local blood flow resulting in areas of rapidly changing blood flow velocities and steep gradients of blood shear rate. Shear rate gradients are known to be pro-thrombotic with an important role for the shear-sensitive plasma protein von Willebrand factor (VWF).

Here, we developed a single-chain antibody (scFv) that targets a shear gradient specific conformation of VWF to specifically inhibit platelet adhesion at sites of SRGs but not in areas of constant shear.

Microfluidic flow channels with stenotic segments were used to create shear rate gradients during blood perfusion. VWF-GPIbα interactions were increased at sites of shear rate gradients compared to constant shear rate of matched magnitude. The scFv-A1 specifically reduced VWF-GPIbα binding and thrombus formation at sites of SRGs but did not block platelet deposition and aggregation under constant shear rate in upstream sections of the channels. Significantly, the scFv A1 attenuated platelet aggregation only in the later stages of thrombus formation. In the absence of shear, direct binding of scFv-A1 to VWF could not be detected and scFV-A1 did not inhibit ristocetin induced platelet agglutination.

We have exploited the pro-aggregatory effects of SRGs on VWF dependent platelet aggregation and developed the shear-gradient sensitive scFv-A1 antibody that inhibits platelet aggregation exclusively at sites of shear rate gradients. The lack of VWF inhibition in non-stenosed vessel segments places scFV-A1 in an entirely new class of anti-platelet therapy for selective blockade of pathological thrombus formation while maintaining normal haemostasis.

Introduction:

Atherothrombotic events precipitating myocardial infarction and ischemic stroke are the most common causes of death worldwide (1). These events are triggered by intraluminal plaque rupture causing an inappropriate platelet response which leads to occlusion of the vessel lumen(2). As a preventative measure, prescribed antiplatelet drugs such as aspirin and clopidogrel target major platelet activation pathways such as the TXA_2- and ADP-$P2Y_{12}$-pathways, thereby reducing platelet reactivity(3). While this is a clinically proven strategy to reduce cardiovascular events, this approach can also cause serious side effects, most notably bleeding, as the targeted pathways also play a critical role in normal haemostasis thereby partly offsetting the benefits gained from these drugs(4-6). Thus, a strategy to uncouple thrombosis from haemostasis to target one without the other is an urgent unmet clinical need.

Platelet aggregates formed during a haemostatic response typically do not grow beyond 50% of the vessel lumen(7, 8), a restriction that is insufficient to markedly change the shear rates at the site of injury(9). However, studies into the haemodynamic regulation of thrombus formation have led to the concept that rapidly changing shear conditions at the site of a cardiovascular insult contribute significantly to the pathological thrombotic response(10, 11). Plaque rupture with its release of highly thrombogenic content may cause the formation of a large thrombus that reduces the vessel lumen which in turn causes local steep increases in blood shear rates, also termed shear rate gradients (SRG). In recent years, the effects of SRG flow patterns on platelet reactivity and von Willebrand factor (VWF) unfolding and activation have been increasingly studied(11-13). VWF is a large blood-borne protein critical to platelet adhesion in areas of high shear such as in arterioles or larger arteries with luminal constriction. In normal circulation, VWF has a globular conformation, which unfolds under high shear stress thereby exposing binding epitopes, most importantly the platelet GPIbα binding domain A1. This unfolding of VWF is referred hereafter as VWF activation.

It is thought that SRGs are one to two orders of magnitude more efficacious in unfolding VWF, compared to constant shear(14, 15). Indeed, we and others have previously demonstrated that shear rate gradients strongly unfold and subsequently activate VWF and that shear gradient dependent platelet aggregation mechanisms promote arterial thrombosis in a VWF-dependent fashion(15, 16).

Given the central role of VWF in platelet adhesion at arterial shear rates, and even more so under pathological flow conditions (i.e. SRG), we hypothesised that activated (i.e. unfolded) VWF is a potential target for a new class of anti-thrombotic therapy.

Here we investigated the effect of SRGs on VWF-mediated platelet adhesion and thrombus formation. Moreover, we report on the generation of the single-chain antibody (scFv) A1, designed to target shear activated VWF. Here, we developed a single-chain antibody (scFv) based on the sequence of parent IgG antibodies raised against the monomeric 39/34-Kd fragment of VWF which encompasses

the VWF-A1 domain and a proximal N-terminal sequence to VWF-A1. Our scFv targets a shear gradient specific conformation of VWF to inhibit VWF-platelet binding specifically at sites of SRGs but not in areas of constant shear.

This antibody specifically inhibits VWF-platelet interactions at pathological shear but not under physiological shear regimens and may therefore form the basis of a new and safer class of anti-thrombotic therapy.

Methods

A more detailed description of the methods is published in the supplementary data.

Single-chain antibody generation

A single chain antibody was designed by combining the variable regions of the light and heavy chains of 2 selected antibodies from a panel of parent IgG antibodies that we raised against a 34/39 kDa fragment of VWF (17).

Blood sampling

Blood samples were collected in trisodium citrate (0.32% w/v final) and immediately processed for further use. The study was approved by the Alfred Hospital's (Melbourne, Australia) ethics committee no 67/15.

Microfluidic chips & *In vitro* flow perfusions

In-house designed PDMS microfluidic chips (Figure 1A) contained channels of 52 µm height with a semi-circular stenotic section, creating 80% lumen reduction. Chips were manufactured as previously reported(16). Citrated whole blood was incubated with $DiOC_6$ (0.5 µg ml^{-1}) (Sigma-Aldrich) and drawn through the microfluidic channels by a programmable syringe pump (Legato 130, KD Scientific) over a coated surface of 100 µg/ml collagen type III or type I.

Computational fluid dynamics and calculations

Fluid dynamics were simulated with a COMSOL Multiphysics 4.2 laminar flow module applied to three-dimensional meshes. For all simulations, no-slip boundary conditions and Newtonian fluids were assumed. Both the computational fluid dynamical simulation and the calculations of fluid dynamical and geometrical parameters were carried out with the assumption that the channels and vessels were filled with Newtonian fluids. This assumption is valid because the shear rates are in a regime in which the non-Newtonian behaviour of blood is limited (18).

Platelet agglutination

Platelet agglutination in response to 0.75 mg mL^{-1} ristocetin (Helena Biosciences, Gateshead, UK) was performed for 10 min on an AggRam system from Helena Laboratories, USA. Isolated platelets (150 or 300 µL at 3 x 10^8/ml) and platelet poor plasma (50 µl) were incubated with 2, 2.5, 4, 5, 40 and 80 µg ml^{-1} scFv A1.

Western Blot

Denatured full-length VWF (Mybiosource, USA) was electrophoresed at 0.1, 10, 100 ng and 1 µg using 5% SDS-Polyacrylamide gel at 125 V for 90 min. The protein was transferred onto PVDF membrane at 90V for 90 min followed by incubation with 1 µg ml^{-1} scFv A1 overnight and the membrane was probed with horse-radish peroxidase (HRP)-conjugated detection antibody (1:2500,

Sigma). Later, the membrane was stripped and reprobed with 1 μg ml^{-1} polyclonal sheep anti-VWF antibody (Abcam), followed by donkey anti-sheep HRP-conjugated secondary antibody (1:2500, R&D Systems, USA).

ELISA

Purified full-length VWF or isolated A1 domain was coated at 0.1, 1 and 10 μg ml^{-1} in the presence of ristocetin (0.75 mg ml^{-1}) and blocked with 2% BSA followed by incubation with 5 μg ml^{-1} of scFv A1 or sheep anti-VWF antibody and detection by HRP-conjugated secondary antibody

BLItz

Bio-layer Interferometry was performed on a BLItz System (Pall Forte Bio, USA) using Protein-A biosensors tagged with VWF-A1 domain (130 μg ml^{-1}). Remaining binding sites were blocked by exposure to a polyclonal mouse IgG for 5 min. Sequential adhesion of scFv-A1 at 0, 20, 40 and 100 μg ml^{-1} was monitored for 5 min per concentration.

Results:

SRGs activate VWF and reduce platelet rolling velocity on VWF/collagen type III

As previously reported(16) exacerbated thrombus formation at atherosclerotic geometries is dependent on the degree of intraluminal sidewall protrusion which creates SRGs. Thus, to elucidate the underlying mechanism of exacerbated thrombus formation under SRGs, platelet adhesion and VWF-activation were studied at sites of SRGs utilising a microfluidic platform. These channels exhibit a stenotic feature which resembled rheological parameters in larger carotid arteries in humans (i.e. slope of stenosis, wall shear rates at the inlet versus stenotic region, and maximal flow elongational rate) while keeping required blood volume low(16). Channels incorporated a semi-circular stenotic geometry of 600 μm in length to reduce the channel width by 80 % from 300 μm to 60 μm (Figure 1A). Computational fluid dynamic analysis indicated that the wall shear rate was symmetrically distributed around the stenosis, with an 8-fold higher shear rate in the apex region compared with the pre-stenotic segment. At an input wall shear rate of 300 s^{-1}, platelets travelling through the stenosis are therefore exposed to an increase in shear rate to 2,400 s^{-1} and a shear gradient (Δs^{-1}) of approximately 7.1 s^{-1} μm^{-1} followed by an identical shear decrease in the outlet of the stenosis (Figure 1B).

Platelet rolling velocities, a measure of VWF-GPIbα bond strength, were reduced at SRGs (assessed in a 140 μm zone around the apex of the stenosis with a maximal shear rate of 2,400 s^{-1}) compared to matched constant wall shear rate of 2,400 s^{-1} (3.9±0.2 μm s^{-1} vs 5.4±0.7 μm s^{-1}) (Figure 1C), with 52.9±2.5 % of slow-rolling platelets at SRGs compared to 36±5.7 % at constant shear (Figure 1D).

This finding indicates that shear rate gradients reduce platelet translocation, presumably through the unfolding of the VWF-A1 domain leading to stronger VWF-GPIb interactions. To confirm this finding, platelet surface coverage, a measure of VWF-platelet interaction was measured in stenotic channels over a wide range of input shear rates ranging from 125 s^{-1} to 8,000 s^{-1}, resulting in shear rates of 1,000 s^{-1} to 36,000 s^{-1} in the stenosis apex and SRGs of approximately 3 s^{-1} μm^{-1} to 1000 s^{-1} μm^{-1}. SRGs facilitated higher levels of transient platelet adhesion, with maximal platelet adhesion of 20.1±3.4 % at 2,500 s^{-1} and sustained platelet adhesion up to 7,000 s^{-1}, (7.89±1.86%; p=0.0462) while platelet adhesion rapidly decreased under constant shear from a maximum of 19.3±1.9 % at 875 s^{-1} and was abolished above 2,000 s^{-1} (13.6±2.0%; p=0.0341) (Figure 1E).

To elucidate the parameters critical for platelet-VWF interaction under SRG, VWF deposition onto collagen type III was tested under either static conditions or under flow in the absence of SRGs. Following VWF deposition onto collagen, the coated strips were overlaid with micro-channels featuring straight or stenotic sections. Platelet rolling velocities at SRGs or constant shear rate (CSR) were assessed at an effective wall shear rate of 2,400 s^{-1}. The rolling velocity of platelets on collagen strips that were statically incubated with VWF was higher (SRG: 5.03±0.31 µm s^{-1}; CSR: 5.44±0.2 µm s^{-1}) than those in channels incubated with VWF at a shear rate of 1,000 s^{-1} (SRG: 4±0.26 µm s^{-1}; CSR: 3.95±0.21 µm s^{-1}, $p<0.05$) (Figure 1F) indicating a role for flow in VWF deposition to collagen. However, when VWF was bound to collagen before platelet perfusion, the SRG specific increase of the GPIbα-VWF bond strength was lost (Figure 1F), suggesting that VWF deposition needs to occur under real-time SRGs to have subsequently increased engagement of GPIbα.

To test the effect of the steepness of the stenosis gradient on platelet rolling velocity, channels containing different stenotic segment lengths were manufactured. These ranged from 600 to 2000 µm in length, resulting in the same peak shear rate in the apex, but different shear rate gradients, ranging from 7.1 s^{-1} μm^{-1} to 3.2 s^{-1} μm^{-1} (Figure 1G). Interestingly, platelet rolling velocities correlated with the magnitude of SRGs. Rolling velocities were negatively correlated with the stenosis gradient, producing the slowest rolling velocity (4.32±0.23 µm s^{-1}) when travelling through a 600 µm stenosis and the highest (5.89±0.35 µm s^{-1}) when travelling through a 2,000 µm stenosis. However, the rolling velocity in the absence of SRG (i.e. under constant shear) was still higher (6.72±0.28 µm s^{-1}) (Figure 1H).

To confirm that previously observed platelet-surface interactions in our experimental setup were exclusively mediated through VWF-GPIbα, blood was incubated with the GPIbα inhibitor OS-1(19). Blood perfusion at a shear rate of 1,500 s^{-1} resulted in platelet adhesion of 74.2±19.5 AU which was concentration-dependently reduced by OS-1. Platelet adhesion was completely abolished in the presence of 3 µM OS-1 (Figure 2A). Furthermore, inhibition of platelet GPIbα by OS-1 (3 µM) caused a sharp decrease in numbers of adherent platelets from above 500 s^{-1} (53±4 platelets per field) to 2,000 s^{-1} (11±4 platelets per field) (Figure 2B).

Having demonstrated that the observed interaction was GPIbα-VWF dependent with only minor if any contribution of direct collagen III interaction above 500 s^{-1}, we tested whether platelet activation played a role in the observed differential rolling velocity. Thus, platelets were treated with aspirin plus the $P2Y_{12}$ inhibitor 2-MeSAMP. The drug treatment did not affect rolling velocity at sites of SRG (Figure 2D), nor at constant shear (Figure 2C), highlighting that the observed rolling velocity on collagen III is solely determined by the biophysical interaction of GPIbα with VWF independent of platelet activation.

Single-chain antibody A1 specifically inhibits SRGs-dependent platelet-VWF interaction

SRGs have been shown to strongly activate VWF, which promotes platelet deposition at pathological shear rates thereby exacerbating thrombus formation. Specifically blocking SRG-mediated VWF-activation would potentially open up a new avenue of limiting excessive thrombus growth at the latter stages of atherothrombosis, thereby keeping the blood vessels patent.

To investigate whether SRG-activated VWF is a potential therapeutic target, we produced several scFvs, based on the sequences of the variable heavy and light chain regions derived from a panel of mAbs raised against a 34/39 kDa VWF fragment incorporating the VWF A1 domain. The new scFvs were specifically tested for their capacity to inhibit VWF-platelet interactions selectively at sites of SRG. ScFv A1 reduced platelet-VWF adhesion specifically in the stenosis inlet, where shear gradients are the greatest from 6187±1097 platelets/mm^2 to 5158±1032 platelets/mm^2; p=0.0013 (Figure 3A). No differences in platelet adhesion were observed at the apex (3934±892 platelets/mm^2 control; 3805±783 platelets/mm^2 scFv A1, p=0.7932); nor in the stenosis outlet (5042±1167 platelets/mm^2 control; 4475±1199 platelets/mm^2 scFv A1; p=0.07). Surprisingly, scFv A1 showed an opposite effect in the straight section under constant shear, leading to increased platelet-deposition (2047±232 platelets/mm^2 control; 3096±690 platelets/mm^2 scFv A1; p=0.0195) (Figure 3A). Platelet rolling velocities were largely unaffected by the addition of scFv A1 except for the stenosis apex where a mild increase in rolling velocity was observed upon addition of scFv A1 (4.41±0.1 μm s^{-1} control; 4.6±0.1 μm s^{-1} scFv A1; p=0.038) (Figure 3B). The relative amount of VWF per platelet deposited on aggregates in areas of SRGs and constant shear was not reduced by scFv A1 (Figure 3C). Taken together these data suggest that scFv A1 interferes with a soluble fraction unfolded VWF which prevents VWF from engaging with surface-bound platelets.

ScFv A1 specifically inhibits shear rate gradient-exacerbated thrombus formation

Taking the findings of the effect of scFv A1 on platelet rolling velocity and adhesion further into a more complex scenario, we tested its capacity to specifically inhibit SRG-mediated thrombus formation. Blood containing scFv A1 (5 μg ml^{-1}) or control antibody was drawn through stenosis channels coated with collagen type I. ScFv A1 had no effect on platelet deposition at constant shear in

the straight channel sections (figure 4A, left panel). To highlight the differences in growth rate between constant shear and shear rate gradients, the aggregate sizes over time were normalized to those measured at 1 min into the flow (set as t=0 in the graph) and defined as relative thrombus growth. Relative thrombus growth under constant shear ranged from 2.11±0.23 vs. 1.9±0.36 at 2,000 s^{-1} to 1.48±0.16 vs. 1.62±0.2 at 1,500 s^{-1} (Figure 4B, left panels). However, under SRG conditions, scFv A1 significantly reduced thrombus formation from 1.85±0.28 to 1.17±0.07 ($p<0.0001$) at 2,000 s^{-1} and from 1.58±0.22 to 1.2±0.09 ($p<0.001$) at 1,500 s^{-1} (Figure 4B, right panels). Inhibition of thrombus formation by scFv A1 was absent at a dose of 2.5 µg ml^{-1} whereas 5 and 10 µg ml^{-1} showed inhibition and to a similar degree (Supplementary figure 1).

Next, the inhibitory effects of ScFv A1 were compared to the platelet GPIbα inhibitor OS-1 after 15 minutes of blood flow. Addition of 0.1 µM OS-1, a concentration that allowed residual platelet adhesion as determined in Figure 2A, inhibited platelet deposition under both constant and shear gradient conditions (Figure 4C). At 2000 s^{-1} constant shear OS-1 reduced thrombus formation from while scFv A1 had no effect. A similar pattern, although weaker, was observed at 1,500 s^{-1}. In contrast, at SRGs (300-2,000 s^{-1}) and (187-1,500 s^{-1}), both OS-1 and scFv A1 inhibited thrombus formation. These data highlight the shear selective nature of ScFV A1 compared to a generic GPIb-VWF inhibitor.

ScFv A1 does not interact with VWF under no shear conditions.

Next we investigated whether scFv A1 could also inhibit VWF-GPIb binding under zero shear conditions. VWF dependent platelet agglutination was tested in a ristocetin-induced platelet agglutination test (RIPA). Since the exposure of VWF to ristocetin or shear reportedly exposes similar epitopes within VWF(20), we hypothesized that scFv A1 may inhibit ristocetin stimulated platelet agglutination. However, scFv A1 up to 80 µg ml^{-1} (16 times higher than used in the microfluidic flow device) did not result in delayed or reduced agglutination of isolated platelets by ristocetin (0.75 mg ml^{-1}) in the presence of plasma VWF. However, when plasma VWF was preincubated with scFv A1 and ristocetin to facilitate their interaction before platelet binding, a minor inhibitory effect of scFv A1 on platelet agglutination was observed (Supplementary Figure S2A). Western blotting of denatured VWF with scFv A1 also did not show any complex formation (Supplementary Figure S2B). Similarly, scFv A1 did not bind to immobilized full-length VWF or isolated VWF A1 domain in an ELISA test (Supplementary Figure S2C). Consistent with this result, we also did not observe any binding between immobilized VWF-full length or VWF-A1 domain with scFv using the BLItz binding assay (Supplementary Figure S2D).

ScFv A1 dampens thrombus formation in the latter stages only.

During the growth of an intraluminal thrombus, the local shear environment becomes progressively more complex. Here we set out to mimic this highly dynamic process and characterize the inhibitory

effects of scFv A1 within this process. Large platelet aggregates were allowed to form in straight channels and create their own local shear gradient environment during thrombus growth. Whole blood was perfused at 1,000 s^{-1} over discrete patches of coated collagen type I surrounded by albumin coated areas (Fig 5A). The presence of the albumin-collagen interface generates a sharp front of aggregates which grow to significant heights relative to the 52µm high channels and as a result create a local steep shear gradient. After an initial phase of homogenous platelet accumulation across the entire collagen patch, platelet aggregation progressively increased at the front area of the patch (2.0±0.2-fold increase; front over rear) (Figure 5B). This effect could not be explained by depletion of platelets at the boundary layer as it was observed on sequential patches within a single channel. Next, we tested scFv A1 for its capacity to inhibit thrombus formation in this progressive shear gradient flow model. ScFv A1 selectively attenuated platelet aggregation at the front area of the collagen patch (Figure 5C) however, scFv A1 did not reduce platelet aggregation in the rear area where shear rates were constant and SRGs were absent. CFD analysis of a representative experiment revealed that platelet aggregates at the front area of the patch experienced increased surface shear rates compared to those in the back area of the patch (Fig 5D; upper panel), concomitant with platelet deposition patterns. As expected, scFv A1 reduced platelet deposition at the front area resulting in reduced aggregate surface shear rates (Figure 5D; lower panel). The inhibitory effect of scFv A1 was observed even though the calculated maximum shear rate gradient, expressed as s^{-1}/µm, was lower in this flow model (4.9 and 3.1 s^{-1}/µm for control and scFv A1 respectively) compared to the SRGs calculated in the microfluidic stenosis channels used in Figures 1-4 (7.1 s^{-1}/µm) (Fig 5D).

Time-lapse confocal microscopic analysis of platelet aggregate formation across the collagen patch revealed a lag phase of up to 180 seconds where small aggregates formed throughout the patch, followed by a growth phase at the front area of the patch where scFv A1 was inhibitory (Figure 5E). Indeed, quantitative analysis showed that scFv A1 inhibited platelet aggregation only at the front of the patch but not at the rear (Fig. 5F).

Discussion:

In this study, we demonstrate that SRGs exacerbate VWF-dependent platelet aggregation through increased VWF-GPIbα bond strength and that this process can selectively be inhibited using an antibody strategy that targets a SRG-sensitive epitope within the VWF A1-domain. Thus, SRGs are a potential novel drug target for the prevention of occlusive thrombus formation.

The blood flow dynamics in areas of flow restriction, stenosis or mural thrombus formation have long been known to create gradients in shear rate, or SRGs. However, the activating effects of SRGs on VWF-dependent platelet aggregation are still largely unknown. We have previously demonstrated the potential of micro-shear gradients in promoting thrombus formation(10). Following on from this finding, we have shown exacerbated thrombus formation in the outlet of stenotic vessel sections to be VWF dependent(16). While high constant shear in the range of approximately 5,000 s^{-1} to 8,000 s^{-1} is required to unfold and thereby activate VWF(14), SRGs dramatically reduce this shear range by 10-fold. This means SRG mediated platelet aggregation can occur in virtually all vessel beds where a flow constriction occurs. Previous studies investigating the role of the VWF-GPIbα axis in platelet adhesion and aggregation used various approaches ranging from mathematical simulations(21, 22), single molecule force probe pulling(23, 24), VWF multimer analysis(25) to functional platelet adhesive behaviour under flow conditions(26-28). However, it is difficult to establish functional links between these studies and, in isolation, they provide limited insight into the overall mechanism of VWF mediated platelet aggregation under shear conditions, particularly SRGs. In our study, we used CFD analysis for the characterisation of our microfluidics setup, linking the shear profile to functional readouts such as platelet aggregate formation, platelet adhesion and rolling velocity as a direct consequence of SRG induced VWF unfolding and activation.

First, we investigated the effects of shear rate gradients on individual platelet-surface interactions on a collagen type III matrix because this type of collagen shows high affinity for VWF, resulting in high VWF density, while causing mild platelet activation. To prevent engagement of αIIbβ3 with VWF during platelet adhesion/aggregation, whole blood was preincubated with the αIIbβ3-inhibitor abciximab. Next, we investigated the effects of shear rate gradients on platelet aggregation on a collagen type I matrix because this type of collagen induces strong platelet activation and subsequent aggregate formation. Most importantly, the use of collagen I or III as a physiological VWF substrate, rather than glass-immobilized VWF, ensured correct conformation of shear-immobilised VWF(29, 30).

Our data show that platelet rolling velocities at SRGs are lower than at matched constant shear, suggesting that SRGs at the inlet of the stenosis, lead to a rapid unfolding of VWF beyond the degree expected under matched constant shear. This unfolding promotes the formation of catch bonds between VWF and GPIbα and reduces the rolling velocity of platelets on the adhesive surface either

due to a higher degree of unfolding per VWF molecule or more unfolded VWF molecules in general. In analogy to tether formation in platelets(28), this feature of SRGs may arrest a platelet sufficiently long to facilitate firm adhesion to the adhesive surface or a neighbouring platelet, thereby exacerbating thrombus formation under SRGs.

Common antiplatelet drugs - aspirin plus a $P2Y_{12}$ inhibitor - did not prevent the pro-adhesive phenotype of platelets under SRG conditions, highlighting that platelet activation does not play a key role in SRG mediated platelet adhesion and that current antiplatelet therapy would be unable to inhibit exacerbated thrombosis which is induced by mechanical hyper-activation of VWF by SRGs.

Others have identified the GPIbα-VWF axis as a potential target and various drug candidates are currently under investigation (31). In contrast to our SRG-specific approach, these drugs take a systemic approach, thereby potentially affecting haemostasis. We sought an approach that would allow inhibition of VWF specifically at sites of SRGs, a feature of atherothrombosis, without affecting VWF-activation under constant shear, which prevails during normal haemostasis.

Our blocking strategy contained the novel scFv A1, which was based on the sequences from a previously developed human mAB panel raised in mice against a 39/34-kDa VWF fragment (Leu-480/Val-481–Gly-718) which encompasses the A1 domain and a sequence N-terminal to that(17). The basis for the generation of our single-chain antibody scFv A1 involved combining the variable heavy chain of an antibody which recognizes a linear epitope in VWF-A1 with the variable light chain of another antibody which recognises a conformation-specific epitope in the VWF A1 domain(17).

Assessing single platelet binding to the adhesive surface, our scFv A1 showed selective platelet-VWF inhibition at stenotic sites where SRGs are prevalent compared to areas of constant shear suggesting that the scFv A1 did not systemically block the VWF-GPIbα interaction but rather specifically at the stenosis and in a transient manner. Similarly, under constant shear conditions platelet aggregation on collagen-bound VWF in the presence of scFv A1 was not inhibited. Taken together, these results suggest that scFv A1 targets the transiently present hyperactive form of VWF at the site of a stenosis. In agreement with this, the presence of hyperactive VWF at sites of SRGs has previously been reported*(16)*.

The activation state of VWF during the flow immobilization to collagen or immobilized platelets appeared to modulate the subsequent recruitment of additional platelets. When VWF was deposited onto collagen before the flow experiment, SRGs did not exert this pro-adhesive effect on platelets, indicating that the activation state of VWF in the fluid phase at the moment of deposition onto collagen or immobilized platelets is a key determinant in the pro-thrombotic phenotype of SRGs. Similar observations have recently been reported by Receveur et al (32) who used a flow model which introduced SRGs of the same magnitude as those used in this study. VWF unfolding in an accelerating flow field is likely to be very transient, with apparent rapid refolding in areas downstream of SRGs

where shear rates resume a constant level again. Therefore, the binding of scFv A1 to VWF is an elusive event that could only be achieved under shear gradient forces in the microfluidic flow assays. Indeed, we were unable to establish evidence of scFv A1 binding to VWF in other assays with no shear being present, likely due to the epitope for scFv A1 being shielded or not in a correct conformation. Since SRG are thought to be mechanistically similar to very high constant shear, we aimed to mimic the shear unfolding of VWF with the biochemical modulator ristocetin. This antibiotic is known to modulate the VWF-GPIb interaction, binding similar epitopes to those exposed by elevated shear (20). After optimizing experimental conditions for platelet agglutination, scFv A1 inhibited ristocetin-induced platelet agglutination in a minor way suggesting that ristocetin may expose epitopes in VWF that are recognized by scFv A1. Although ristocetin-treated VWF exposes similar epitopes as shear stress, we cannot claim that the topology of the epitopes is the same under both conditions, particularly because we create SRG conditions whereas the literature is based on constant shear rates. This likely explains why the inhibitory effect of our scFv-A1 in the ristocetin induced aggregation assays was only modest and requires further investigations.

One limitation of this study is its exclusive *in vitro* approach to address these questions. The scFv A1 antibody recognizes human VWF and thus would require a fully humanized mouse model of the VWF-GPIb axis to study the efficacy of the antibody in an *in vivo* setting. These *in vivo* approaches will be addressed in subsequent studies. Therapeutic development would include full humanisation of the scFv replacing structural elements that are murine based. Current humanisation technologies are based on decades of experience with antibody scaffolds and in the majority of cases the antibodies keep their properties. However, there is always a small risk that the properties will change and the antibody might become less affine or specific. In case this is observed further affinity maturation might be required which ultimately could make the antibody more potent. A scFv typically clears the circulation in 1/2 hour compared to days of a full IgG antibody. The ultimate clinical application (acute treatment of thrombosis vs prophylaxis) will determine which format is optimal. There might be scope to a fast and slow clearing antibody alone or in combination as required based on the desired pharmacokinetics.

In conclusion, we have shown that pro-thrombotic effects of SRGs, which are known to lead to "hyperactivation" of VWF (32-35) can be site-specifically inhibited with our scFv A1 antibody without interfering with the VWF-GPIbα interaction under normal flow. We speculate that our targeting strategy could provide an important cornerstone in future antithrombotic therapy which mechanically decouples thrombosis from haemostasis and therefore does not contribute to an increased bleeding tendency, one of the main culprits in current antiplatelet drug development.

Acknowledgements:

We are grateful to Monash micro imaging for their technical assistance for the use of confocal microscopes. We thank P. Lenting (INSERM, U1176, France) for providing the plasmids encoding the VWF-FL and VWF-A1 domains.

Source of Funding:

This work was supported by grants from the National Health and Medical Research Council and the National Heart Foundation. H.A. was funded by the European Research Council under the Advanced Grant 'VESCEL' Program (Grant no. 669768)

Disclosures:

Conflict of interest disclosures: The molecular design and sequence of said single-chain antibody scFv-A1 is subject to a patent application (provisional patent no. 2020902148) and is therefore not disclosed in this manuscript.

References:

1. Wang H, Wolock TM, Carter A, et al. Estimates of global, regional, and national incidence, prevalence, and mortality of HIV, 1980-2015: the Global Burden of Disease Study 2015. Lancet HIV. 2016;3(8):e361-387.
2. Robbie L, Libby P. Inflammation and atherothrombosis. Ann N Y Acad Sci. 2001;947:167-179; discussion 179-180.
3. Hoefer T, Armstrong PC, Finsterbusch M, et al. Drug-Free Platelets Can Act as Seeds for Aggregate Formation During Antiplatelet Therapy. Arterioscler Thromb Vasc Biol. 2015;35(10):2122-2133.
4. Antithrombotic Trialists' Collaboration. Collaborative meta-analysis of randomised trials of antiplatelet therapy for prevention of death, myocardial infarction, and stroke in high risk patients. BMJ. 2002;324(7329):71-86.
5. Wallentin L, Becker RC, Budaj A, et al. Ticagrelor versus clopidogrel in patients with acute coronary syndromes. N Engl Med. 2009;361(11):1045-1057.
6. Wiviott SD, Braunwald E, McCabe CH, et al. Prasugrel versus clopidogrel in patients with acute coronary syndromes. N Engl J Med. 2007;357(20):2001-2015.
7. oude Egbrink MG, Tangelder GJ, Slaaf DW, Reneman RS. Thromboembolic reaction following wall puncture in arterioles and venules of the rabbit mesentery. Thromb Haemost. 1988;59(1):23-28.
8. Sixma JJ, Wester J. The hemostatic plug. Semin Hematol. 1977;14(3):265-299.
9. Bark DL, Jr., Ku DN. Wall shear over high degree stenoses pertinent to atherothrombosis. J Biomech. 2010;43(15):2970-2977.
10. Nesbitt WS, Westein E, Tovar-Lopez FJ, et al. A shear gradient-dependent platelet aggregation mechanism drives thrombus formation. Nat Med. 2009;15(6):665-673.
11. Springer TA. von Willebrand factor, Jedi knight of the bloodstream. Blood. 2014;124(9):1412-1425.
12. Zhu S, Herbig BA, Li R, et al. In microfluidico: Recreating in vivo hemodynamics using miniaturized devices. Biorheology. 2015;52(5-6):303-318.
13. Zheng Y, Chen J, Lopez JA. Flow-driven assembly of VWF fibres and webs in in vitro microvessels. Nat Commun. 2015;6:7858.
14. Schneider SW, Nuschele S, Wixforth A, et al. Shear-induced unfolding triggers adhesion of von Willebrand factor fibers. Proc Natl Acad Sci U S A. 2007;104(19):7899-7903.
15. Sing CE, Alexander-Katz A. Elongational flow induces the unfolding of von Willebrand factor at physiological flow rates. Biophys J. 2010;98(9):L35-37.
16. Westein E, van der Meer AD, Kuijpers MJ, et al. Atherosclerotic geometries exacerbate pathological thrombus formation poststenosis in a von Willebrand factor-dependent manner. Proc Natl Acad Sci U S A. 2013;110(4):1357-1362.
17. De Luca M, Facey DA, Favaloro EJ, et al. Structure and function of the von Willebrand factor A1 domain: analysis with monoclonal antibodies reveals distinct binding sites involved in recognition of the platelet membrane glycoprotein Ib-IX-V complex and ristocetin-dependent activation. Blood. 2000;95(1):164-172.
18. Chien S, Usami S, Dellenback RJ, et al. Blood viscosity: influence of erythrocyte aggregation. Science. 1967;157(3790):829-831.
19. Benard SA, Smith TM, Cunningham K, et al. Identification of peptide antagonists to glycoprotein Ibalpha that selectively inhibit von Willebrand factor dependent platelet aggregation. Biochemistry. 2008;47(16):4674-4682.
20. Dong JF, Berndt MC, Schade A, et al. Ristocetin-dependent, but not botrocetin-dependent, binding of von Willebrand factor to the platelet glycoprotein Ib-IX-V complex correlates with shear-dependent interactions. Blood. 2001;97(1):162-168.
21. Sing CE, Selvidge JG, Alexander-Katz A. Von Willlebrand adhesion to surfaces at high shear rates is controlled by long-lived bonds. Biophys J. 2013;105(6):1475-1481.
22. Shiozaki S, Takagi S, Goto S. Prediction of Molecular Interaction between Platelet Glycoprotein Ibalpha and von Willebrand Factor using Molecular Dynamics Simulations. J Atheroscler Thromb. 2016;23(4):455-464.

23. Wijeratne SS, Botello E, Yeh HC, et al. Mechanical activation of a multimeric adhesive protein through domain conformational change. Phys rev Lett. 2013;110(10):108102.
24. Aponte-Santamaria C, Huck V, Posch S, et al. Force-sensitive autoinhibition of the von Willebrand factor is mediated by interdomain interactions. Biophys J. 2015;108(9):2312-2321.
25. Groot E, Fijnheer R, Sebastian SA, de Groot PG, Lenting PJ. The active conformation of von Willebrand factor in patients with thrombotic thrombocytopenic purpura in remission. J Thromb Haemost. 2009;7(6):962-969.
26. Savage B, Sixma JJ, Ruggeri ZM. Functional self-association of von Willebrand factor during platelet adhesion under flow.Proc Natl Acad Sci U S A. 2002;99(1):425-430.
27. Maxwell MJ, Dopheide SM, Turner SJ, Jackson SP. Shear induces a unique series of morphological changes in translocating platelets: effects of morphology on translocation dynamics. Arterioscler thromb Vasc Biol. 2006;26(3):663-669.
28. Dopheide SM, Maxwell MJ, Jackson SP. Shear-dependent tether formation during platelet translocation on von Willebrand factor. Blood. 2002;99(1):159-167.
29. Kang I, Raghavachari M, Hofmann CM, Marchant RE. Surface-dependent expression in the platelet GPIb binding domain within human von Willebrand factor studied by atomic force microscopy. Thromb Res. 2007;119(6):731-740.
30. Raghavachari M, Tsai H, Kottke-Marchant K, Marchant RE. Surface dependent structures of von Willebrand factor observed by AFM under aqueous conditions. Colloids Surf B Biointerfaces. 2000;19(4):315-324.
31. Firbas C, Siller-Matula JM, Jilma B. Targeting von Willebrand factor and platelet glycoprotein Ib receptor. Exp Rev Cardiovasc Ther. 2010;8(12):1689-1701.
32. Receveur N, Nechipurenko D, Knapp Y, et al. Shear rate gradients promote a bi-phasic thrombus formation on weak adhesive proteins, such as fibrinogen in a VWF-dependent manner. Haematologica. 2019 Nov 14. [Epub ahead of print]
33. Springer TA. Biology and physics of von Willebrand factor concatamers. J Thromb Haemost. 2011;9 Suppl 1(0 1):130-143.
34. Vergauwe RM, Uji IH, De Ceunynck K, et al. Shear-Stress-Induced Conformational Changes of von Willebrand Factor in a Water-Glycerol Mixture Observed with Single Molecule Microscopy. J Phys Chem B. 2014;118(21):5660-5669.
35. Colace TV, Diamond SL. Direct observation of von Willebrand factor elongation and fiber formation on collagen during acute whole blood exposure to pathological flow. Arterioscler Thromb Vasc Biol. 2013;33(1):105-113.

Figure legends:

Figure 1. SRGs increase VWF-GPIb bond strength and reduce platelet rolling velocity. (A) Complex flow dynamics were studied in microfluidics exhibiting a semi-circular stenotic site with a diameter of 600 µm which reduced the channel width from 300 µm to 60 µm. (B) Computational fluid dynamics identified the stenosis apex as a zone with an eight-fold increase in shear compared to the inlet, followed by a negative but equal drop in shear rate in the stenosis outlet. (C) Abciximab-treated (20 µg ml^{-1}), citrated whole blood, labelled with 0.5 µg ml^{-1} $DiOC_6$ was perfused over a collagen III-coated surface to promote binding of blood borne VWF under flow and subsequent platelet adhesion. Input shear rate was set to 300 s^{-1} which then increased to 2,400 s^{-1} in the apex of the stenosis. Control channels with straight walls were used to generate a constant shear rate of 2,400 s^{-1}. Data represented as mean±SEM; n=8; * $p<0.05$ (unpaired t-test). (D) Platelet rolling velocity on VWF-collagen III was assessed at SRGs (platelets rolling through the apex of the stenotic site) or constant shear (upstream of the stenotic site) using particle tracking software. Platelet rolling velocities were divided into three bins (0-3 µm s^{-1}; >3-6 µm s^{-1}; >6 µm s^{-1}) and presented as relative frequencies. Data represented as mean±SEM; n=5; * $p<0.05$ (multiple unpaired t-tests). (E) Surface coverage of abciximab-treated, citrated whole blood, labelled with $DiOC_6$ perfused over a collagen III-coated surface. Input shear rates ranged from 125 s^{-1} up to 8,000 s^{-1} for stenotic channels, resulting in peak shear rates of 1,000 s^{-1} to 36,000 s^{-1} in the apex of the stenosis; or matched shear rates in a parallel control channel exhibiting a constant shear rate throughout. (F) Collagen type III-coated channels were incubated either statically or perfused at 1,000 s^{-1} or 10,000 s^{-1} with platelet poor plasma in the absence of SRG to allow VWF adhesion to collagen. Abciximab-treated, citrated whole blood, labelled with $DiOC_6$ was perfused over the differentially coated collagen III/VWF matrix as described in (B). Platelet rolling velocity on VWF / collagen III was assessed at SRGs (platelets rolling through the apex of the stenotic site) or constant shear (upstream of the stenotic site) for all 3 coating regimens using particle tracking software. Data represented as mean±SEM; n=3; * $p<0.05$ (multiple unpaired t-tests) (G) Abciximab-treated, citrated whole blood, labelled with $DiOC_6$ was perfused over a collagen III matrix, through 300 µm wide channels incorporating semi-circular stenotic segments which reduced the channel width to 60 µm. The diameters of semi-circular stenotic elements ranged from 600 µm and 1,000 µm to 2,000 µm. Whereas Δ shear of all three stenotic segments was equal, levels of elongational flow differed. (H) Platelet rolling velocity on VWF-collagen III was assessed the same conditions as in (C) under SRGs (platelets rolling through the apex of the stenotic site) or constant shear (upstream of the stenotic site) using particle tracking software. Data represented as mean±SEM; n=3; * $p<0.05$ (Dunnett's multiple comparison one-way ANOVA).

Figure 2. Platelet adhesion to collagen III is VWF-GPIb dependent. (A) Blood, containing $DiOC_6$-labelled platelets, was treated with increasing concentrations of OS-1. Blood samples were drawn through collagen III coated channels at 1,500 s^{-1}. Fluorescence intensity was measured and expressed as relative platelet adhesion. (B) Citrated whole blood treated with 20 µg ml^{-1} Abciximab and 3 µM OS-1 was perfused through collagen III-coated microfluidics at constant shear rates ranging from 125 s^{-1} to 2,000 s^{-1}. Data represented as mean±SEM; n=4; * $p<0.05$ (Dunnett's multiple comparison one-way ANOVA). (C) Abciximab-treated (20 µg ml^{-1}) platelets were treated with DAPT (30µM aspirin plus 300 µM 2-MeSAMP) or control and drawn through stenotic or straight channels. Platelet rolling velocity on collagen III bound VWF was assessed under constant shear (C) and at SRGs (D) using particle tracking software. Rolling velocities were divided into three bins (0-3 µm s^{-1}; >3-6 µm s^{-1}; >6 µm s^{-1}) and presented as relative frequencies (C, D) Data represented as mean±SEM; n=3; * $p<0.05$ (multiple unpaired t-tests).

Figure 3. Single-chain antibodies scFv A1 differentially inhibits VWF-platelet interaction at constant shear or gradients of shear (A) Abciximab-treated (20 µg ml^{-1}), citrated whole blood, labelled with 0.5 µg ml^{-1} $DiOC_6$ containing scFv A1 (5 µg ml^{-1}) or control was perfused over a collagen III-coated surface as described in figure 1B. Platelet adhesion was assessed at the stenosis inlet, apex, outlet and upstream areas using particle tracking software. Data represented as matched individual data points and mean±SEM; n=5; * $p<0.05$. (C) Relative VWF amount corrected for the level per platelet in platelet aggregates under SRGs and constant shear. Data represented as mean±SEM; n=3-4; (multiple t-test).

Figure 4 scFv A1, but not OS-1 selectively inhibits thrombus formation in stenotic channel segments, a site of SRGs, but not at constant shear rate.

Confocal microscopy images of platelet aggregates (A) and quantification (B) of aggregate growth. Citrated whole blood, labelled with 0.5 µg ml^{-1} $DiOC_6$, containing 5 µg ml^{-1} scFv A1 (black) or control (red), was perfused over a collagen type I matrix for 10 minutes at an effective shear rate of 1,500 and 2,000 s^{-1} in the stenosis apex (Shear rate gradient) or upstream (constant shear). Note the inhibitory effect of scFv A1 at SRG but not under constant shear. Data represented as mean±SEM; n=3-4; * $p<0.05$ (2-way ANOVA). (C) Confocal images of platelet aggregate formation as in (A) in the presence of the GPIb inhibitor OS-1 (0.1 µM) or control. (D) Quantification of platelet aggregate growth after 15 minutes at sites of SRG or at constant shear in the presence of scFv A1 (5µg/ml), OS-1 (0.1 µM) or control (D). Data represented as mean±SEM; n=3-6; * $p<0.05$ (2-way ANOVA).

Figure 5. scFv A1 specifically inhibits thrombus formation at sites of SRGs but not at constant shear rate. Citrated whole blood, labelled with 0.5 µg ml^{-1} $DiOC_6$, containing 5 µg ml^{-1} scFv A1 or control, was drawn at 1000 s^{-1} through flow channels exhibiting a patch of perpendicularly-coated collagen type I (100 µg ml^{-1}) on the bottom surface, creating a BSA-collagen interface. (A) Z-slices of confocal microscopy images were binarized and compiled to z-projections showing thrombus height for control (top panel) and scFv A1-loaded blood (bottom panel). (B) Relative fluorescence intensities of platelet aggregates on sequential collagen patches in the same flow channel. Data represented as mean±SEM; n=3; *$p<0.05$ (multiple t-tests). (C) Relative fluorescence intensities of platelet aggregates in the front-, centre- and rear areas of the collagen patch after 10 minutes of flow. Data represented as mean±SEM; n=3; *$p<0.05$ (multiple t-tests). (D) CFD analysis of shear rates present at the surface of platelet aggregates in control blood and scFv A1-treated blood, expressed as a heat map and numerical. Maximal shear rate gradients are shown for the microfluidic stenosis channels used in figures 1-4 and at the surface of the aggregates shown in the heat map. (E) Graphical presentation of the platelet fluorescence distribution over the entire collagen patch at various timepoints. Data is mean of n=3 flows. (F) Quantification of time-lapse confocal microscopy images showing reduced platelet deposition in the presence of scFv A1 at the front area but not the rear area of the patch. Data represented as mean±SEM; n=3; * $p<0.05$ (2-way ANOVA).

Figure 1

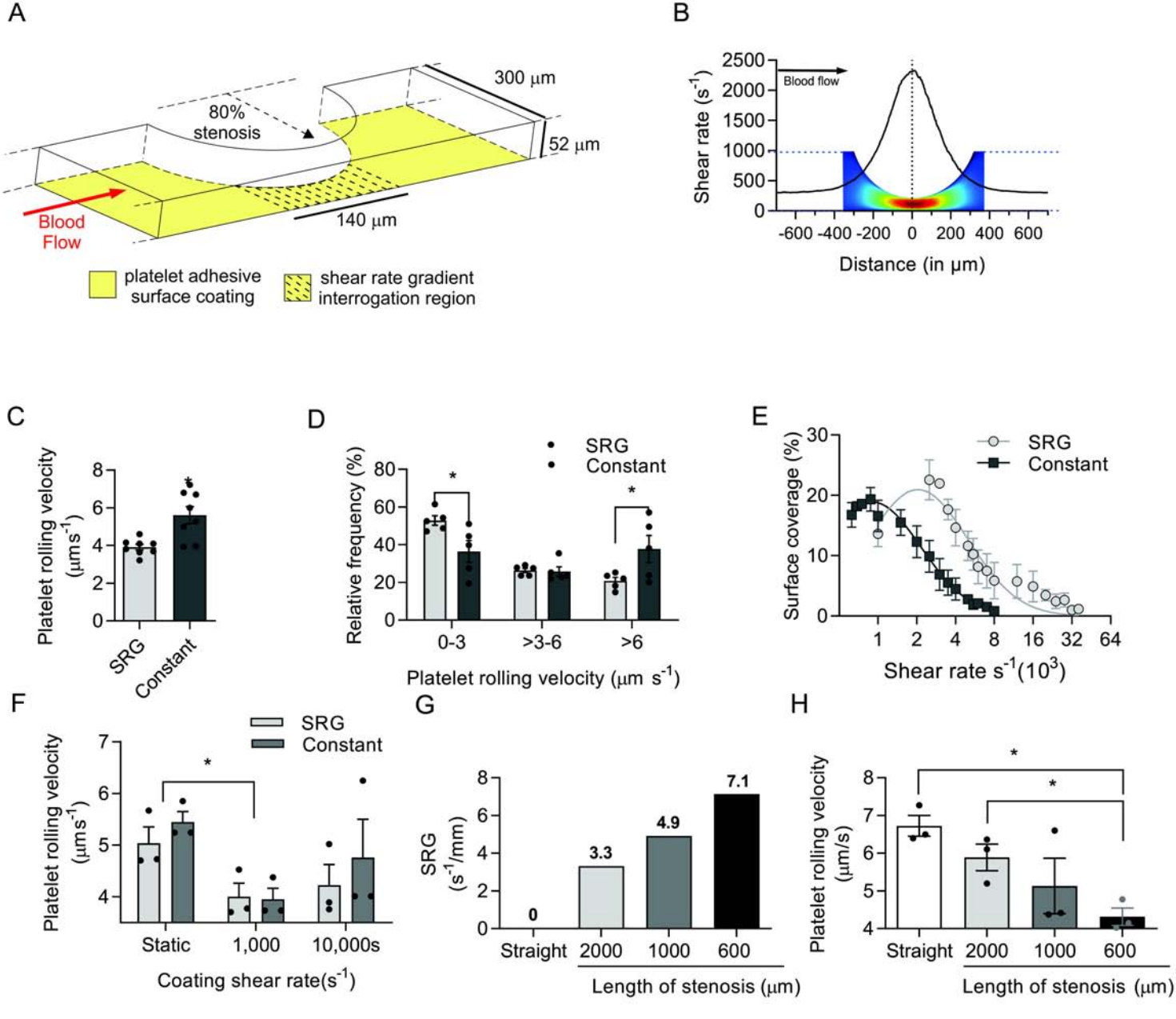
A
300 μm
80% stenosis
52 μm
Blood Flow
140 μm
platelet adhesive surface coating
shear rate gradient interrogation region
B
Blood flow
Shear rate (s-1)
2500
2000
1500
1000
500
0
-600 -400 -200 0 200 400 600
Distance (in μm)
C
Platelet rolling velocity (μms-1)
SRG
Constant
D
SRG
Constant
Relative frequency (%)
0-3
>3-6
>6
Platelet rolling velocity (μm s-1)
E
SRG
Constant
Surface coverage (%)
Shear rate s-1(103)
F
SRG
Constant
Platelet rolling velocity (μms-1)
Static
1,000
10,000s
Coating shear rate(s-1)
G
SRG (s-1/mm)
0
3.3
4.9
7.1
Straight
2000
1000
600
Length of stenosis (μm)
H
Platelet rolling velocity (μm/s)
Straight
2000
1000
600
Length of stenosis (μm)

Figure 2

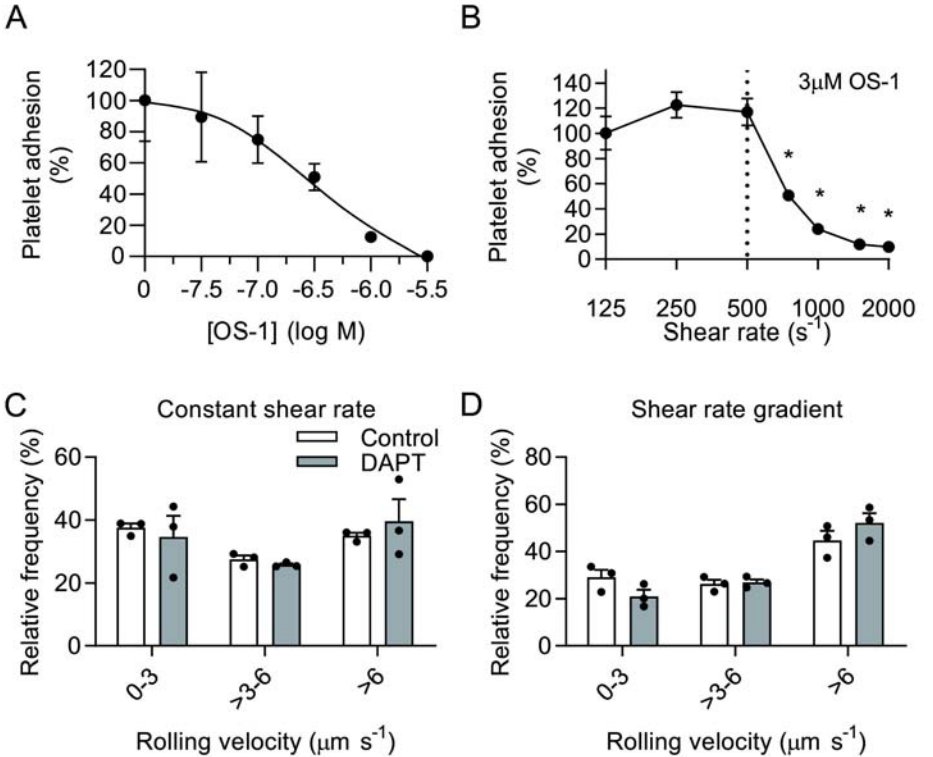
A
Platelet adhesion (%)
120
100
80
60
40
20
0
0
-7.5
-7.0
-6.5
-6.0
-5.5
[OS-1] (log M)
B
Platelet adhesion (%)
140
120
100
80
60
40
20
0
3μM OS-1
*
*
*
*
125
250
500
1000
2000
Shear rate (s-1)
C
Constant shear rate
Control
DAPT
Relative frequency (%)
60
40
20
0
0-3
>3-6
>6
Rolling velocity (μm s-1)
D
Shear rate gradient
Relative frequency (%)
80
60
40
20
0
0-3
>3-6
>6
Rolling velocity (μm s-1)

Figure 3

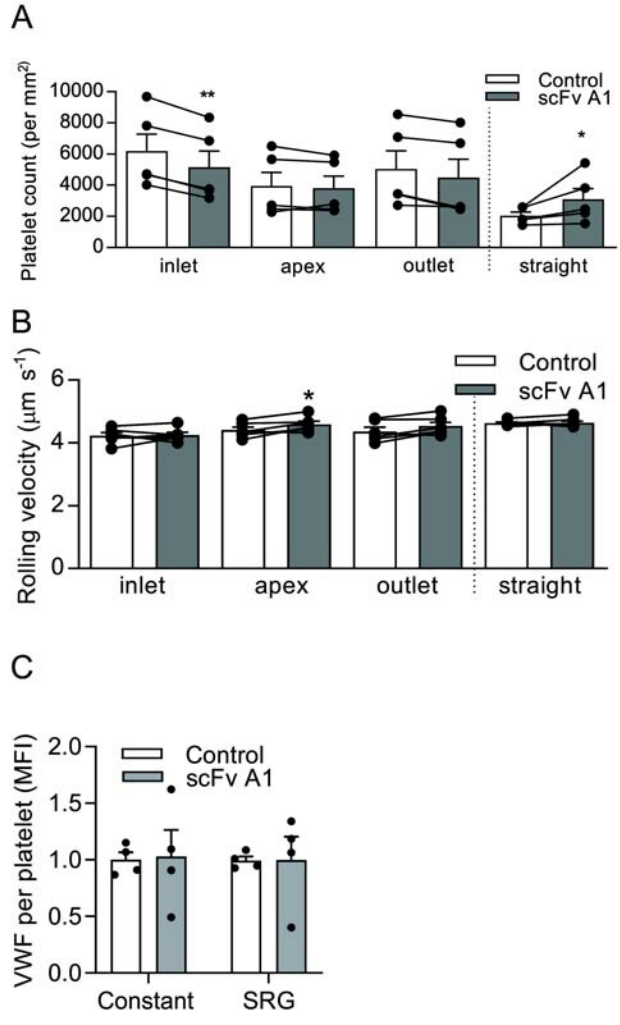
A
Platelet count (per mm2)
10000
8000
6000
4000
2000
0
**
*
Control
scFv A1
inlet
apex
outlet
straight
B
Rolling velocity (μm s-1)
6
4
2
0
*
Control
scFv A1
inlet
apex
outlet
straight
C
VWF per platelet (MFI)
2.0
1.5
1.0
0.5
0.0
Control
scFv A1
Constant
SRG

Figure 4

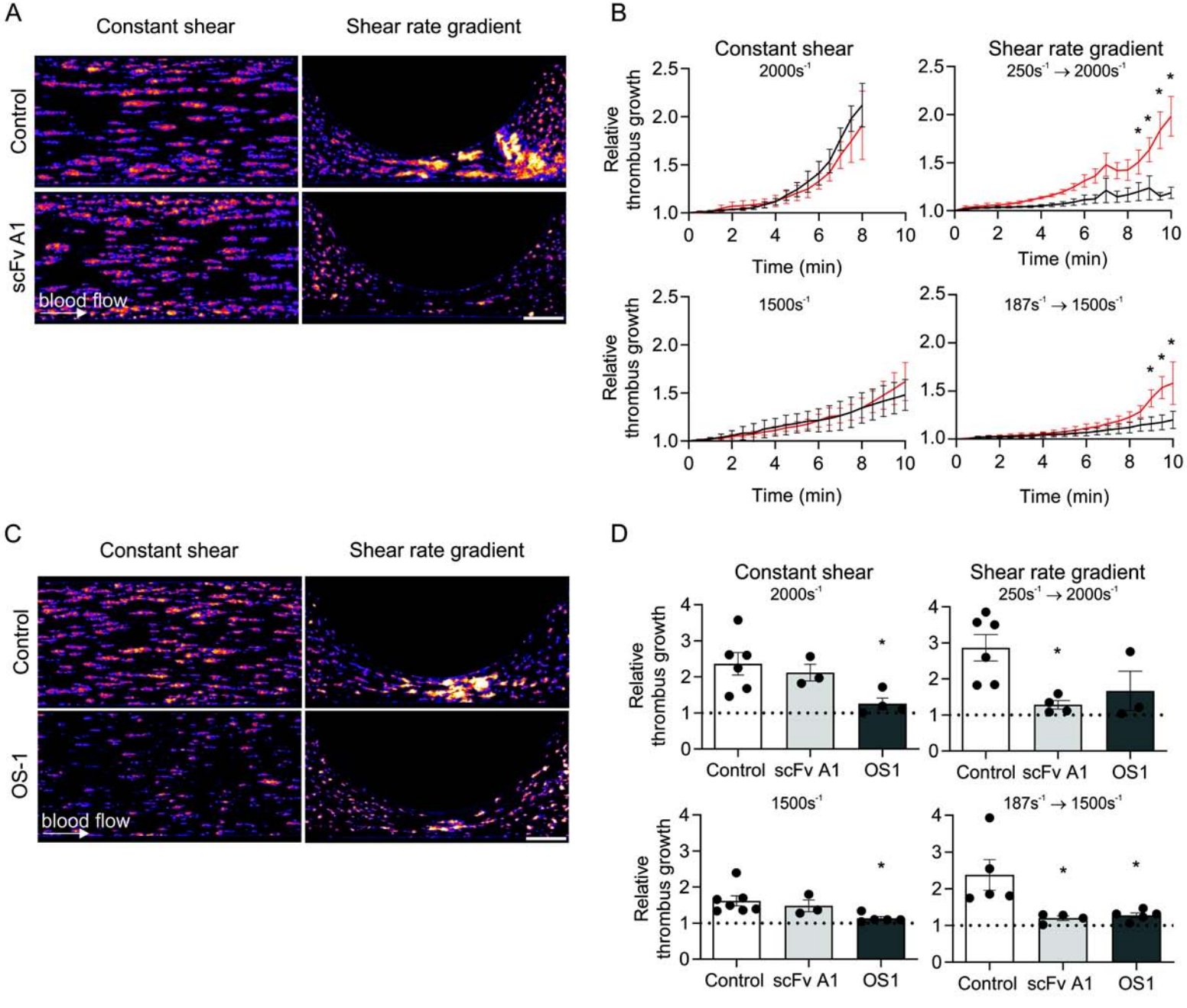
A
Constant shear
Shear rate gradient
Control
scFv A1
blood flow
B
Constant shear
2000s-1
Shear rate gradient
250s-1 → 2000s-1
Relative thrombus growth
Time (min)
1500s-1
187s-1 → 1500s-1
C
Constant shear
Shear rate gradient
Control
OS-1
blood flow
D
Constant shear
2000s-1
Shear rate gradient
250s-1 → 2000s-1
Relative thrombus growth
Control
scFv A1
OS1
1500s-1
187s-1 → 1500s-1

Figure 5

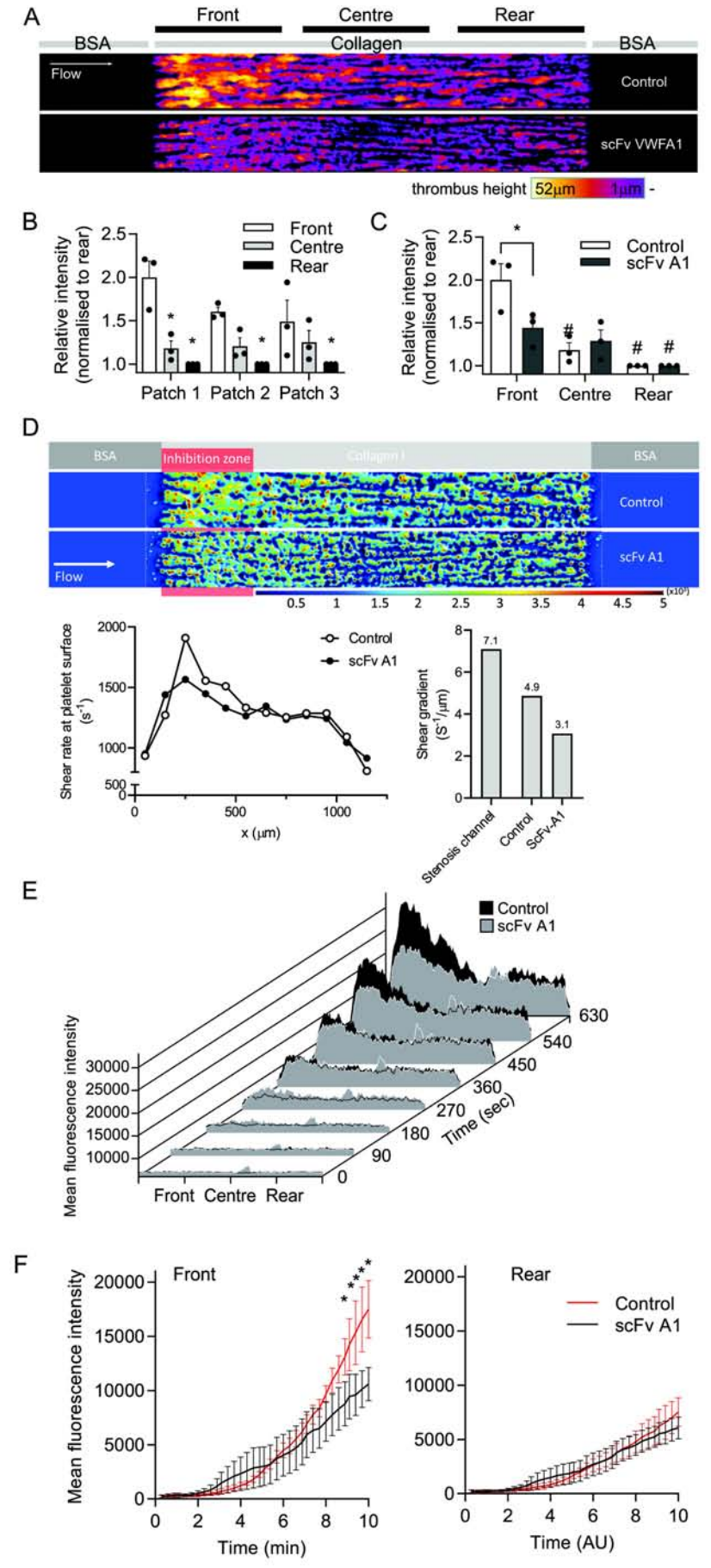
A
Front
Centre
Rear
BSA
Collagen
BSA
Flow
Control
scFv VWFA1
thrombus height 52µm 1µm
B
Relative intensity (normalised to rear)
Front
Centre
Rear
Patch 1
Patch 2
Patch 3
C
Relative intensity (normalised to rear)
Control
scFv A1
Front
Centre
Rear
D
BSA
Inhibition zone
Collagen I
BSA
Control
scFv A1
Flow
Shear rate at platelet surface (s-1)
x (µm)
Control
scFv A1
Shear gradient (S-1/µm)
7.1
4.9
3.1
Stenosis channel
Control
ScFv-A1
E
Control
scFv A1
Mean fluorescence intensity
Front Centre Rear
Time (sec)
F
Front
Rear
Mean fluorescence intensity
Time (min)
Time (AU)
Control
scFv A1

Supplementary method and results

Targeting shear gradient activated von Willebrand Factor by the novel single-chain antibody A1 reduces occlusive thrombus formation in vitro.

Thomas Hoefer[1*], Akshita Rana[2*], Be'eri Niego[2], Shweta Jagdale[1,2], Hugo J. Albers[3,4], Elizabeth E. Gardiner[5], Robert K. Andrews[2], Andries D. van der Meer[3], Christoph E. Hagemeyer[1,2**]& Erik Westein[1,2**]

[1]Baker Heart and Diabetes Institute, Melbourne, Australia;
[2]Australian Centre for Blood Diseases, Monash University, Melbourne, Australia;
[3]Applied Stem Cell Technologies, University of Twente, Enschede, The Netherlands;
[4]BIOS Lab-on-a-Chip, University of Twente, Enschede, The Netherlands;
[5]ACRF Department of Cancer Biology and Therapeutics, John Curtin School of Medical Research, Australian National University, Canberra, Australia

Methods and materials:

Single-chain antibody generation

A panel of IgG antibodies was previously raised in mice against a 34/39 kDa fragment incorporating the human VWF A1 domain and a sequence N-terminal to that (1). The sequence of the light and heavy chains was determined as described before(2). Briefly, mRNA was prepared and reverse transcribed using an oligo-dT primer. The variable regions of the antibody's heavy and light chains were amplified by polymerase chain reaction (PCR) using primers that anneal to conserved regions at the 5' and 3' ends of the variable regions and sequenced. The variable regions of the light and heavy chains of 2 antibodies from this panel were combined with a standard linker sequence and various tags added for purification and bioconjugation purposes (FLAG-tag, a HIS-tag and a sortase reaction site). The derived DNA-sequences were ordered from a commercial supplier (Geneart, Invitrogen) optimized for the final host expression system, cloned into a pSec-tag vector, expressed using a HEK293 cell line and purified as described before(3, 4). In brief, after confirmation of the final clone, DNA was transfected with polyethylenimine (Polyscience Inc.) into human HEK293 kidney cells. After transfection, cells were cultured for 7 days at 37°C, with 5% CO_2, shaking at 140 rpm. The supernatant was collected and purified with a nickel-based metal affinity chromatography column, Ni-NTA column (Qiagen), according to the manufacturer's instructions. Purified scFv was dialysed against PBS at 4°C overnight. The cyclic peptide, OS-1 which is an allosteric

inhibitor of GPIbα/VWF interactions with sequence CTERMALHNLC was obtained from Auspep (Parkville, Australia)

Blood sampling

The study was approved by the Alfred Hospital's (Melbourne, Australia) ethics committee no 67/15 and all volunteers gave written consent. The volunteers abstained from aspirin, non-steroidal anti-inflammatory drugs (NSAIDs) and any other anti-platelet therapy for 10 days before blood was taken from the median cubital vein using a 21G butterfly needle and collected into vacuette tubes (Sarstedt AG & Co, Nuembrecht, Germany) containing trisodium citrate (0.32% w/v final). Blood samples were immediately processed for further use.

Microfluidic chips

In-house designed PDMS microfluidic chips (Figure 1A) contained channels of 52 µm height with a footprint of 300 µm x 46 mm (used in figure 1) or 300 µm x 17 mm. Selected channels incorporated a semi-circular stenotic section of various lengths (600 µm, 1000 µm or 2000 µm diameter), creating 80% lumen reduction. Chips were manufactured as previously reported(5). The produced PDMS chips were sealed with cover slips by hydrophobic interaction and coated with collagen by perfusion of collagen solution followed by static incubation at RT for at least 1 hr. Channels were rinsed with PBS and blocked with 2% BSA. Wall shear rates of the input flow for these microchannels were approximated from volumetric flow rates by using the equation, $\gamma = 6Q/wh^2$. Herein, γ is the wall shear rate (s^{-1}), Q the volumetric flow rate (mls^{-1}), w the channel with (cm) and h the channel height (cm).

Computational fluid dynamics and calculations

Fluid dynamics were simulated with a COMSOL Multiphysics 4.2 laminar flow module applied to three-dimensional meshes. For all simulations, no-slip boundary conditions and Newtonian fluids were assumed. To obtain meshes from the plain channel geometries, channel dimensions were taken from the original computer-aided design (CAD) files and reconstructed in COMSOL. To obtain meshes from platelet aggregate geometries, confocal fluorescence microscopy image z-stacks of labelled platelets were processed in ImageJ. Each image in a z-stack was converted into a binary image by thresholding, and an x-y heightmap was constructed by summing all binary data in a z-stack followed by multiplying the result with the height of the original z-stack as documented by the confocal microscope. These heightmaps were imported in COMSOL to construct three-dimensional meshes. Input flow parameters

were set based on pump settings as used in the experiments, and were adjusted to account for the reduced width of the fluorescence aggregate meshes compared to the full channel geometries. Both the computational fluid dynamical simulation and the calculations of fluid dynamical and geometrical parameters were carried out with the assumption that the channels and vessels were filled with Newtonian fluids. This assumption is valid because the shear rates are in a regime in which the non-Newtonian behaviour of blood is limited (6)(6).

***In vitro* flow perfusions**

Citrated whole blood was incubated with $DiOC_6$ (0.5 µg ml^{-1}) (Sigma-Aldrich Co, St. Louis, MO, USA) and drawn through microfluidic channels by a programmable syringe pump (Legato 130, KD Scientific, USA). Time-lapse z-stack images of platelet deposition were captured in multiple track, resonant scanning mode, using a Nikon A1R confocal microscope system. Platelet deposition was recorded over time (2 frames per minute) for up to 20 minutes and quantified in ImageJ using a Z-projection of the acquired signal.

For experiments measuring rolling velocities, anti IIb3 antibody (abciximab; 20 µg ml^{-1})-treated whole blood containing 0.5 µg ml^{-1} $DiOC_6$ was drawn over a collagen type III-coated surface. Where indicated, blood was incubated with 30 µM aspirin and 300 µM 2-MeSAMP (Sigma-Aldrich) before blood perfusion. 10-second video clips of rolling platelets were recorded in the green fluorescent channel using an Olympus IX81 microscope system. Platelet rolling velocities were calculated using Diatrack v3.04 large scale particle tracking software(7).

Platelet agglutination

Platelet rich plasma (PRP) was obtained from citrated whole blood by centrifugation at 300 x g for 10 min and further centrifugation at 1700 x g for 7 min to obtain platelet-poor plasma (PPP; source of plasma VWF). Isolated platelets (3 x 10^8/ml) suspended in platelet wash buffer (4.3 mM K_2HPO_4, 4.3 mM Na_2HPO_4, 24.3 mM NaH_2PO_4, 113 mM NaCl, 5.5 mM D-glucose, and 10 mM theophylline, pH 6.5) were centrifuged at 1500 x g for 7 min. The washed platelets were subsequently resuspended at the same concentration in modified Tyrode's buffer (10 mM Hepes, 12 mM $NaHCO_3$, 137 mM NaCl, 2.7 mM KCl and 5 mM glucose, pH 7.3) containing calcium (1 mM), magnesium (1 mM) and apyrase (0.02 U ml^{-1}) (ADPase activity). Isolated platelets (150 or 300 µL at 3 x 10^8/ml) and platelet poor plasma (50 µl) were incubated with 2, 2.5, 4, 5, 40 and 80 µg ml^{-1} scFv A1 and the corresponding concentration of control scFv or

Tyrode's buffer. αIIbβ3 (GPIIb/IIIa) blocker, Eptifibatide (Integrilin) was used to neutralise any other aggregation mechanisms besides the VWF A1-GPIbα interaction. Platelet agglutination in response to 0.75 mg mL^{-1} ristocetin (Helena Biosciences, Gateshead, UK) was performed for 10 min on an AggRam system from Helena Laboratories, USA

Western Blot

Denatured full-length VWF (Mybiosource, USA) was electrophoresed at 0.1, 10, 100 ng and 1 µg using 5% SDS-Polyacrylamide gel at 125 V for 90 min. The protein was transferred onto PVDF membrane at 90V for 90 min followed by incubation with 1 µg ml^{-1} scFv A1 overnight and the membrane was probed with horse-radish peroxidase (HRP)-conjugated detection antibody (1:2500, Sigma). Later, the membrane was stripped and reprobed with 1 µg ml^{-1} polyclonal sheep anti-VWF antibody (Abcam), followed by donkey anti-sheep HRP-conjugated secondary antibody (1:2500, R&D Systems, USA). Chemiluminescent detection of protein bands was done using ECL Western Blotting Substrate (ThermoFisher) and visualisation using a ChemiDoc Touch Imaging system (Bio-Rad, UK).

ELISA

ELISA wells (Thermo Fisher Scientific) were coated with purified full-length VWF or isolated A1 domain at 0.1, 1 and 10 µg ml^{-1} in the presence of ristocetin (0.75 mg ml^{-1}) and blocked with 2% BSA. Next, the coated wells were incubated with 5 µg ml^{-1} of scFv A1 or sheep anti-VWF antibody followed by incubation with an HRP-conjugated secondary antibody (Anti-his HRP for scFv A1, Donkey anti-sheep HRP antibody for sheep anti-VWF antibody) (1:4,000). Readings were measured at 450 nm on a BMG Optima multi-well reader.

BLItz

Bio-layer Interferometry was performed on a BLItz System (Pall Forte Bio, USA). Protein-A biosensors were hydrated for 30 minutes in PBS-Tween (0.05%) and loaded with Fc-tagged VWF-A1 domain (130 µg ml^{-1}). Remaining binding sites were blocked by exposure to a polyclonal mouse IgG for 5 min. Sequential adhesion of scFv-A1 at 0, 20, 40 and 100 µg ml^{-1} was monitored for 5 min per concentration. Real-time visualisation of binding interactions between scFv A1 and full-length VWF/A1 domain was performed using the BLItz Pro software. Traces were manually baseline aligned and corrected for control binding (0 µg ml^{-1} scFv-A1).

Supplementary Figures

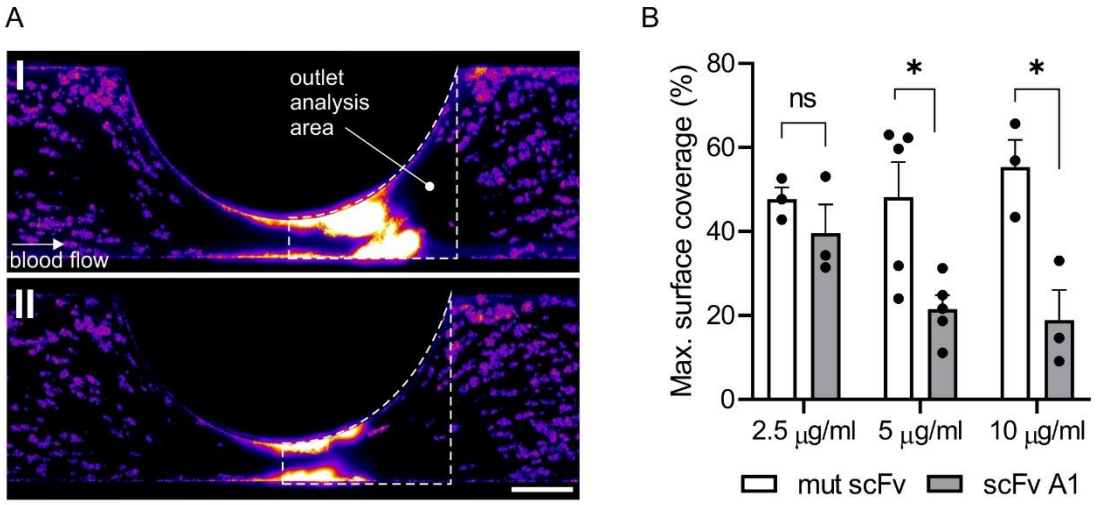

Figure S1. ScFv A1 dose dependently inhibits platelet aggregation at stenotic sites. (A) representative false colour images of platelet aggregate formation in the stenosis outlet region in the presence of (I) control mut-scFV and (II) 10 μg ml^{-1} scFv A1 after 10 minutes of flow at 250s^{-1} input shear rate. (B) Maximum surface coverage measured in the outlet analysis area as shown in (A). Data represented as mean±SEM; n=3-5; *p<0.05 (multiple t-tests).

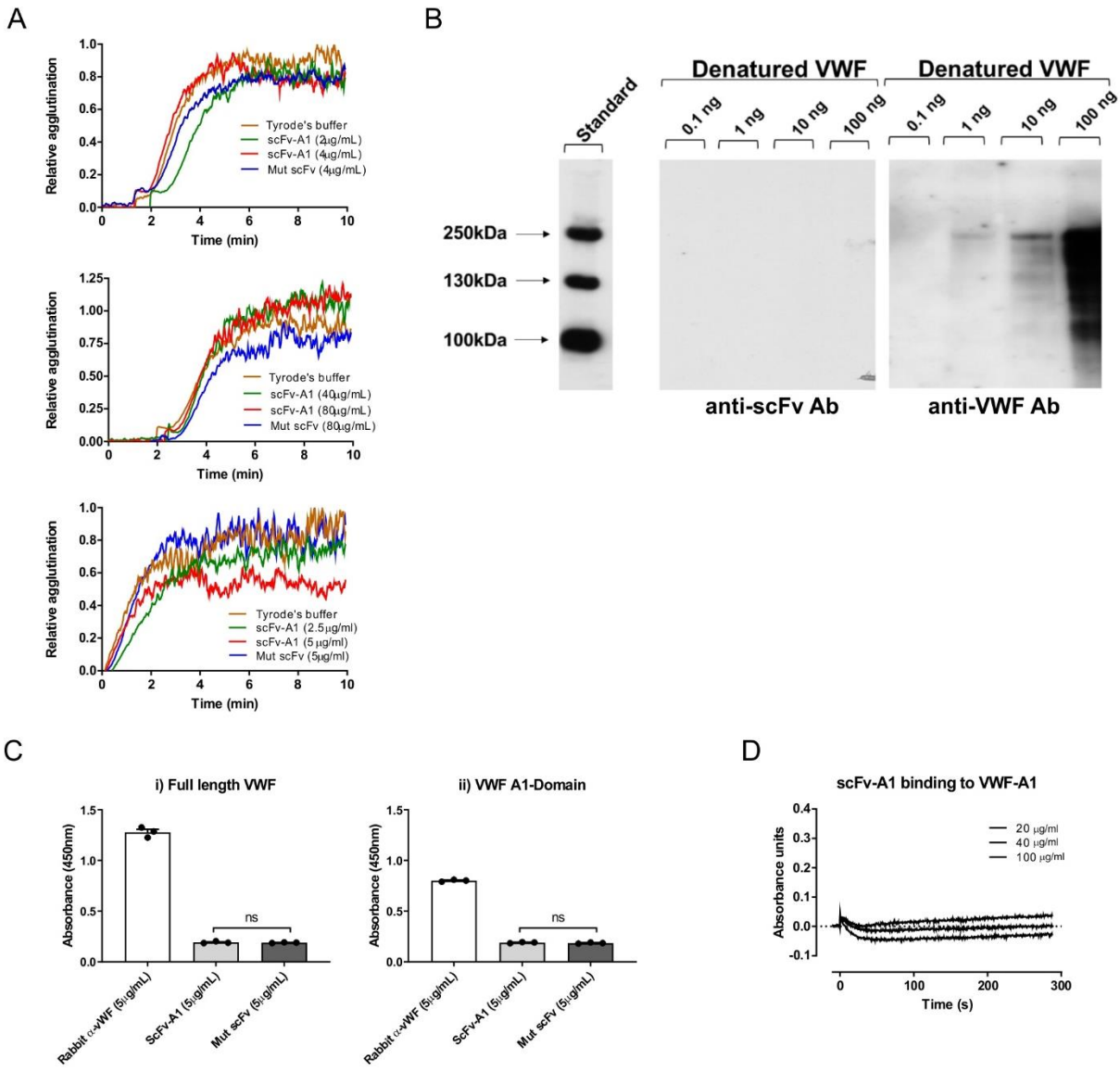

Figure S2. Static assays to characterize the binding of ScFv A1 to VWF. (A) Ristocetin (0.75 mg ml^{-1}) induced platelet agglutination traces. i) 300 µL washed platelets and 50 µL of platelet poor plasma (PPP) treated with 2, 4 µg ml^{-1} scFv A1, Mutated scFv or Tyrode's buffer. ii) 150 µL of isolated platelets, 50 µL of platelet poor plasma (PPP) treated with 40, 80 µg ml^{-1} scFv A1, Mutated scFv or Tyrode's buffer. iii) 50 µL of platelet poor plasma (PPP) preincubated with ristocetin for 30 min before mixing with 150 µL of isolated platelets, treated with 2.5 or 5 µg ml^{-1} scFv A1, control scFv or Tyrode's buffer. Agglutination was recorded for 10 minutes and normalized to Tyrode's buffer sample. (B) Western blot analysis of VWF protein (at 0.1, 10, 100 ng µl^{-1} and 1 µg µl^{-1}) denatured via SDS-PAGE, probed with i) scFv-A1(1 µg ml^{-1}) followed by anti-his HRP antibody (1:2500), ii) sheep α-VWF (1 µg ml^{-1}) antibody followed by donkey α-sheep HRP antibody (1:2500). (C) ELISA absorbance values for binding of 5 µg ml^{-1} scFv-1 A1 or control mut-scFV to i) full-length VWF (10 µg ml^{-1}) in the presence of 0.75 mg ml^{-1} ristocetin , and ii) purified A1 domain (10 µg ml^{-1}). Data are mean±SEM; n=3 (t-test). (D) BLItz association traces for scFv-A1 (20, 40 and 100 µg ml^{-1}) binding to VWF-A1 domain immobilized onto a protein-A BLItz probe. Shown traces are background subtracted using a PBS only sample.

References

1. De Luca M, Facey DA, Favaloro EJ, Hertzberg MS, Whisstock JC, McNally T, et al. Structure and function of the von Willebrand factor A1 domain: analysis with monoclonal antibodies reveals distinct binding sites involved in recognition of the platelet membrane glycoprotein Ib-IX-V complex and ristocetin-dependent activation. Blood. 2000 Jan 1;95(1):164-72.
2. Stoll P, Bassler N, Hagemeyer CE, Eisenhardt SU, Chen YC, Schmidt R, et al. Targeting ligand-induced binding sites on GPIIb/IIIa via single-chain antibody allows effective anticoagulation without bleeding time prolongation. Arteriosclerosis, thrombosis, and vascular biology. 2007 May;27(5):1206-12.
3. Bonnard T, Tennant Z, Niego B, Kanojia R, Alt K, Jagdale S, et al. Novel Thrombolytic Drug Based on Thrombin Cleavable Microplasminogen Coupled to a Single-Chain Antibody Specific for Activated GPIIb/IIIa. J Am Heart Assoc. 2017 Feb 3;6(2).
4. Alt K, Paterson BM, Westein E, Rudd SE, Poniger SS, Jagdale S, et al. A versatile approach for the site-specific modification of recombinant antibodies using a combination of enzyme-mediated bioconjugation and click chemistry. Angew Chem Int Ed Engl. 2015 Jun 22;54(26):7515-9.
5. Westein E, van der Meer AD, Kuijpers MJ, Frimat JP, van den Berg A, Heemskerk JW. Atherosclerotic geometries exacerbate pathological thrombus formation poststenosis in a von Willebrand factor-dependent manner. Proceedings of the National Academy of Sciences of the United States of America. 2013 Jan 22;110(4):1357-62.
6. Chien S, Usami S, Dellenback RJ, Gregersen MI, Nanninga LB, Guest MM. Blood viscosity: influence of erythrocyte aggregation. Science. 1967 Aug 18;157(3790):829-31.
7. Vallotton P, Olivier S. Tri-track: free software for large-scale particle tracking. Microsc Microanal. 2013 Apr;19(2):451-60.